



Dominant modes of CMIP3/5 models simulating northwest Pacific circulation anomalies during post-ENSO summer and their SST dependence

Weichen Tao^{1,2} · Gang Huang^{1,3,4,5} · Pengfei Wang^{1,6} · Yang Liu⁷ · Guanjuan Wen⁸ · Danhong Dong¹

Received: 7 October 2018 / Accepted: 28 June 2019 / Published online: 11 July 2019
© Springer-Verlag GmbH Austria, part of Springer Nature 2019

Abstract

Based on an intermodel empirical orthogonal function (EOF) analysis, this study has investigated the dominant modes of northwest Pacific (NWP) circulation anomalies during post-ENSO summer and their SST dependence involved in 47 Coupled Model Intercomparison Project phase 3 and phase 5 models. The first EOF mode, explaining 33.3% of total intermodel variance, features an anomalous cyclone over the tropical NWP and is controlled by the positive SST anomalies over the equatorial western Pacific (WP). The equatorial WP warming enhances local convection with lower- (upper-) level convergence (divergence), and the anomalous cyclone is a direct Rossby wave response to positive rainfall anomalies there. The second EOF mode, explaining 24.6% of total intermodel variance, is characterized by an anomalous NWP anticyclone (NWPAC). The related SST anomalies show warming in the tropical Indian Ocean (TIO) and equatorial central and eastern Pacific (CEP) and cooling in the NWP. The TIO (CEP) warming induces local wet anomalies, which trigger eastward (westward) Kelvin (Rossby) wave, resulting the adjustment of large-scale circulation. The resultant lower- (upper-) level divergence (convergence) suppresses convection over the NWP, inducing the anomalous NWPAC as a Rossby wave response. The NWP cooling influences NWPAC via positive thermodynamic feedback between local SST and circulation anomalies. Model results further confirm the role of leading mode-related SST anomalies affecting the simulation of NWP circulation.

1 Introduction

Boreal summer is the major rainy season in East Asia, and the East Asian summer monsoon has considerable socioeconomic impacts on this highly populated region. The prominent mode of interannual variation of East Asian summer monsoon is characterized by an anomalous lower-level anticyclone over the northwest Pacific (NWP; Chang et al. 2000; Wang et al. 2008), which is highly dependent on El Niño-Southern

Oscillation (ENSO) activity (Zhang et al. 1996; Wang et al. 2000; Yang et al. 2007; Xie et al. 2009; Stuecker et al. 2013; Hu et al. 2014; Stuecker et al. 2015; Wu et al. 2017a, b; Xie and Zhou 2017). Thus, the NWP anticyclone (NWPAC) is an important circulation system that connects ENSO and East Asian summertime climate (Wu et al. 2003; Wu et al. 2009a; Hu et al. 2012; Chen et al. 2014; Xie et al. 2016; Zhang et al. 2016; Hu et al. 2017; Tao et al. 2017; Dong et al. 2018; Gong et al. 2018a).

✉ Gang Huang
hg@mail.iap.ac.cn

¹ State Key Laboratory of Numerical Modeling for Atmospheric Sciences and Geophysical Fluid Dynamics, Institute of Atmospheric Physics, Chinese Academy of Sciences, Beijing 100029, China

² Earth System Science Interdisciplinary Center, University of Maryland, College Park, MD 20740, USA

³ Laboratory for Regional Oceanography and Numerical Modeling, Qingdao National Laboratory for Marine Science and Technology, Qingdao 266237, China

⁴ Joint Center for Global Change Studies, Beijing 100875, China

⁵ University of Chinese Academy of Sciences, Beijing 100049, China

⁶ Center for Monsoon System Research, Institute of Atmospheric Physics, Chinese Academy of Sciences, Beijing 100029, China

⁷ National Meteorological Centre, China Meteorological Administration, Beijing 100081, China

⁸ Guangzhou Institute of Tropical and Marine Meteorology, China Meteorological Administration, Guangzhou 510640, China

The NWPAC often develops in late fall of the year when El Niño matures (Zhang et al. 1996; Wang et al. 2000; Stuecker et al. 2015; Wu et al. 2017a, b), and persists into the following summer (Wu et al. 2003; Wu et al. 2009a; Xie et al. 2009; Xie et al. 2016; Xie and Zhou 2017). Numerous studies have explored mechanisms for the formation and maintenance of the NWPAC at different phases of El Niño. From El Niño developing fall to decaying spring, the NWPAC develops rapidly (Zhang et al. 1996; Wang et al. 2000; Stuecker et al. 2015; Wu et al. 2017a, b). On one hand, the Rossby wave cyclonic anomalies induced by El Niño-related positive sea surface temperature (SST) anomalies over the equatorial central and eastern Pacific (CEP) advect dry and low moist enthalpy air into the NWP, which drive the NWPAC through suppressed convection (Wu et al. 2017a). Alternatively, Stuecker et al. (2013) and Stuecker et al. (2015) proposed the combination mode, which emphasizes non-linear interactions of atmospheric response to slow evolution of equatorial CEP SST anomalies with the background annual cycle in the rapid growth of NWPAC. On the other hand, the NWPAC is a Rossby wave response to local SST cooling, and the northeasterly wind anomalies at its east flank superimposed on the northeasterly trade winds reinforce initial cold SST anomalies through evaporation, forming a positive thermodynamic feedback between SST and circulation anomalies (Wang et al. 2000; Wang and Zhang 2002; Wu et al. 2017b).

With the decay of equatorial CEP and NWP SST anomalies, the tropical Indian Ocean (TIO) SST gradually warm up due to El Niño-induced atmospheric and oceanic processes (Lau and Nath 1996; Klein et al. 1999; Chiang and Sobel 2002; Xie et al. 2002; Chowdary and Gnanaseelan 2007; Wu et al. 2008; Du et al. 2009; Wu and Yeh 2010; Tao et al. 2014; Tao et al. 2015b; Chowdary et al. 2016), and mainly contribute to the maintenance of NWPAC from El Niño decaying spring to summer (Watanabe and Jin 2002; Yang et al. 2007; Xie et al. 2009; Wu et al. 2010; Yang et al. 2010; Chowdary et al. 2011; Chen et al. 2016; Xie and Zhou 2017). The TIO warming induces a warm tropospheric Kelvin wave response eastward in atmosphere (Yang et al. 2007; Xie et al. 2009; Yang et al. 2010). The resultant northeasterly winds and lower-level divergence suppress convection, and further maintain the NWPAC (Xie et al. 2009). Recently, Xie and Zhou (2017) illustrated that the TIO warming and NWP cooling form the Indo-northwest Pacific Ocean capacitor mode, which anchors the NWPAC.

The abovementioned mechanisms pose a challenge for the coupled ocean-atmosphere general circulation models (CGCMs) to simulate the NWPAC realistically. Based on outputs of the World Climate Research Programme's (WCRP's) Coupled Model Intercomparison Project (CMIP) phase 3 and phase 5 (CMIP3 and CMIP5) models, Tao et al. (2015a) found

that the simulated NWPAC during the post-ENSO summer is weaker and shifts more northward than observations, and this difference is attributed to unrealistic SST anomalies in the equatorial western Pacific (WP). Further analysis using intermodel empirical orthogonal function (EOF) analysis illustrated the two leading modes of NWPAC biases among CMIP5 models (Tao et al. 2018). However, Tao et al. (2018) were based on CMIP5 models, and will the leading modes vary among CMIP3/CMIP5 models? Besides, Tao et al. (2018) focused on exploring the origins of ENSO-related SST biases, and briefly discussed the relationship between NWPAC and SST biases. It is necessary to further study the detailed processes involved in SST biases affecting NWPAC biases. In present study, the dominant modes of simulated NWPAC during the post-ENSO summer and their SST dependence are re-examined by using CMIP3/5 models. Note that there does not show a prominent difference between CMIP3 and CMIP5 models regarding the simulation of ENSO (Bellenger et al. 2014) and Indo-Pacific SST pattern during ENSO decaying phase (Tao et al. 2015a); thus, all models are put together to form a larger ensemble.

The rest of the paper is organized as follows. Data and methodology used are described in Section 2. Section 3 performs statistical diagnoses and numerical experiments to investigate the two leading modes of NWPAC simulations and their SST dependence. Section 4 provides the summary of the main findings.

2 Data and methodology

We use the CMIP3 climate of twentieth century (20C3M) and CMIP5 historical scenario simulations in this study. The 20C3M experiments were conducted based on observed history of anthropogenic and natural forcing from 1900 to 1999, while the CMIP5 historical experiments are from 1870 to 2006. The detailed information can be found in the following web site: <http://cmip-pcmdi.llnl.gov/>. In this study, 30 years of simulations covering 1970–1999 from 15 CMIP3 and 32 CMIP5 models are used and consistent with Tao et al. (2015a). Table 1 lists the names, institutions, and countries of models. Monthly mean outputs are used, including SST, precipitation, 200 hPa geopotential height, 200 hPa winds, and 850 hPa winds. Only one member (“r1i1p1”) of each model simulations is analyzed. The observational and reanalysis datasets include the following: (1) Hadley Centre Sea ICE and Sea Surface Temperature dataset (HadISST) with $1^\circ \times 1^\circ$ horizontal resolution covers the period from January 1870 to the present (Rayner et al. 2003); (2) NOAA's Precipitation Reconstruction (PREC) with $2.5^\circ \times 2.5^\circ$ horizontal resolution covers the period from January 1948 to the present (Chen et al. 2002); (3) Monthly 200 hPa geopotential height, 200 hPa winds, and 850 hPa winds from the NCEP/NCAR reanalysis product with $2.5^\circ \times 2.5^\circ$ horizontal resolution covers the period

Table 1 The CMIP models used in this study. Nos. 1–32 are CMIP5 models and Nos. 33–47 are CMIP3 models

No.	Model name	Institute (country)
1	ACCESS1.0	Commonwealth Scientific and Industrial Research Organisation and Bureau of Meteorology (Australia)
2	BCC-CSM1.1	Beijing Climate Center (China)
3	BCC-CSM1.1-M	
4	CanCM4	Canadian Centre for Climate Modelling and Analysis (Canada)
5	CanESM2	
6	CCSM4	National Center for Atmospheric Research (USA)
7	CESM1-BGC	
8	CESM1-CAM5	
9	CESM1-FASTCHEM	
10	CESM1-WACCM	
11	CMCC-CM	Centre National de Recherches Météorologiques/Centre Européen de Recherche et Formation Avancée en Calcul Scientifique (France)
12	CNRM-CM5	Centre National de Recherches Meteorologiques (France)
13	CSIRO-Mk3.6.0	Commonwealth Scientific and Industrial Research Organisation in collaboration with the Queensland Climate Change Centre of Excellence (Australia)
14	FGOALS-g2	LASG, Institute of Atmospheric Physics, Chinese Academy of Sciences, and CESS, Tsinghua University (China)
15	GFDL-CM3	Geophysical Fluid Dynamics Laboratory (USA)
16	GFDL-ESM2G	
17	GFDL-ESM2M	
18	GISS-E2-R	NASA Goddard Institute for Space Studies (USA)
19	HadGEM2-CC	Met Office Hadley Centre (UK)
20	HadGEM2-ES	
21	INM-CM4	Institute for Numerical Mathematics (Russia)
22	IPSL-CM5A-LR	Institut Pierre Simon Laplace (France)
23	IPSL-CM5A-MR	
24	IPSL-CM5B-LR	
25	MIROC5	Japan Agency for Marine-Earth Science and Technology, Atmosphere and Ocean Research Institute
26	MIROC-ESM	(The University of Tokyo), and National Institute for Environmental Studies (Japan)
27	MIROC-ESM-CHEM	
28	MPI-ESM-LR	Max Planck Institute for Meteorology (MPI-M) (Germany)
29	MPI-ESM-MR	
30	MRI-CGCM3	Meteorological Research Institute (Japan)
31	NorESM1-M	Norwegian Climate Centre (Norway)
32	NorESM1-ME	
33	bccr_bcm2_0	Bjerknes Centre for Climate Research (Norway)
34	cccma_cgcm3_1_t47	Canadian Centre for Climate Modelling and Analysis (Canada)
35	gfdl2_0	Geophysical Fluid Dynamics Laboratory (USA)
36	gfdl2_1	
37	giss_aom	NASA Goddard Institute for Space Studies (USA)
38	giss_model_e_h	
39	giss_model_e_r	
40	fgoals_g1_0	LASG, Institute of Atmospheric Physics, Chinese Academy of Sciences (China)
41	ipsl_cm4	Institut Pierre Simon Laplace (France)
42	miroc3_2_hires	Center for Climate System Research (Japan)
43	miroc3_2_medres	
44	mpi_echam5	Max Planck Institute for Meteorology (Germany)
45	mri_cgcm2_3_2a	Meteorological Research Institute (Japan)
46	near_pcm1	National Center for Atmospheric Research (USA)
47	ukmo_hadgem1	Met Office Hadley Centre (UK)

from January 1948 to the present (Kalnay et al. 1996). All CMIP outputs and observational datasets are interpolated to a uniform $2.5^\circ \times 2.5^\circ$ grid by bilinear interpolation.

The monthly mean climatology is first calculated for the study period. Then, interannual anomalies are computed as the departure from the climatology. This study focuses on the interannual variation, and we perform a 3-month running average to reduce intraseasonal variability and remove the least squares trend in both model outputs and observations to extract interannual signals. Hereafter, any month in the developing years of ENSO is denoted by suffix (0), whereas any month in the decaying years of ENSO is denoted by suffix (1). DJF represents the seasonal mean in December–January–February, and JJA represents the seasonal mean in June–July–August. The Niño3.4 index is defined as SST anomalies averaged over the region $5^\circ \text{ S}–5^\circ \text{ N}$ and $170^\circ–120^\circ \text{ W}$ in D(0)JF(1). The intensity of NWP circulation anomalies is defined as the difference of 850 hPa zonal winds between a southern region ($5^\circ–15^\circ \text{ N}$, $90^\circ–130^\circ \text{ E}$) and a northern region ($22.5^\circ–32.5^\circ \text{ N}$, $110^\circ–140^\circ \text{ E}$), following Wang and Fan (1999). EOF, regression, and correlation analysis are used, and the significance level is estimated based on the standard two-tailed Student’s *t* test. Bias in present study represents the intermodel diversity.

3 Results

3.1 Leading modes of NWPAC biases

Figure 1a, b compares the NWP circulation anomalies during post-ENSO summer in observations and CMIP MME. In observations, an anomalous anticyclone appears over the NWP (Fig. 1a), while the NWPAC is much weaker with more

northward shift in CMIP MME (Fig. 1b). Besides, CMIP MME simulates significant westerly anomalies over the equatorial WP, due to the unrealistic SST anomalies there (Tao et al. 2015a; Jiang et al. 2017; Tao et al. 2018). Furthermore, the intensity of NWP circulation anomalies in observations, CMIP MME, and each CMIP model are shown in Fig. 1c. The anomalous NWP circulation exhibits large intermodel diversity among CMIP models. Most models simulate weaker NWPAC than observations, and even cyclones rather than anticyclones appear over the NWP in some models, resulting weaker NWPAC in CMIP MME than observations (Fig. 1b, c). To examine the intermodel spread of NWPAC simulations, an intermodel EOF analysis is applied to the 850 hPa wind anomalies during post-ENSO summer over the NWP ($10^\circ \text{ S}–40^\circ \text{ N}$, $90^\circ \text{ E}–170^\circ \text{ W}$) for 47 CMIP models. Figure 2a–d shows the regression of ENSO-related SST, 850 hPa wind, and precipitation anomalies during JJA(1) with respect to the leading two PCs as well as the PCs. The variances explained by the first two EOF patterns are well separated according to North et al. (1982). The leading modes obtained by using CMIP3/5 models in present study are consistent with those of CMIP5 models only (Fig. 2 of Tao et al. 2018).

The first intermodel EOF mode (EOF1), explaining 33.3% of total variance, exhibits a meridional dipole structure of circulation anomalies from the tropical WP to NWP (Fig. 2b). There is an anomalous cyclone located over the tropical NWP, and an anomalous anticyclone appears at its northeast side. Correspondingly, significant positive SST anomalies can be seen over the equatorial WP (Fig. 2a). The relationship between PC1 and WP SST anomalies is further documented in Fig. 3a, and the correlation coefficient between them is 0.82 exceeding 99% significant level. Thus, for EOF1

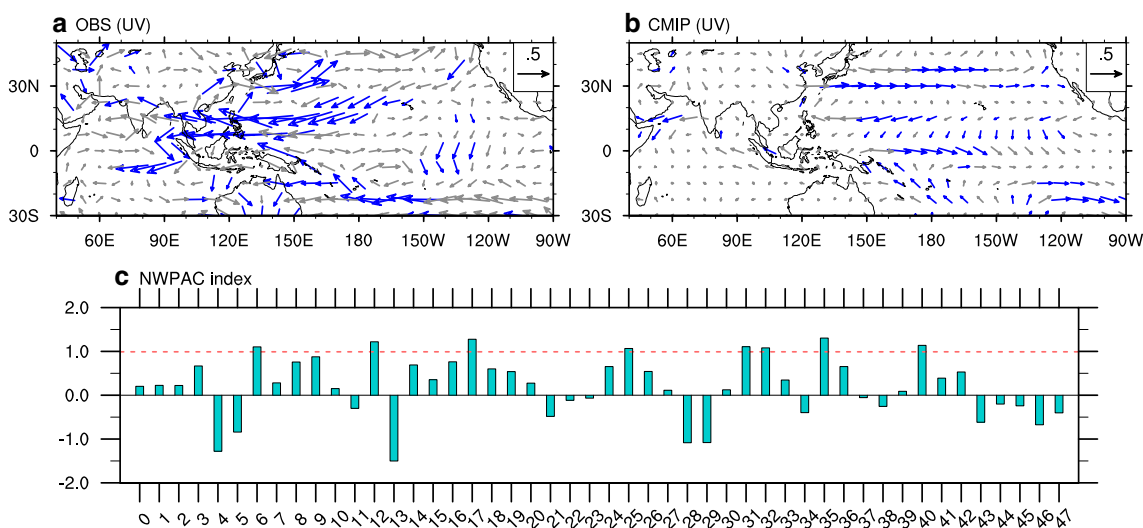


Fig. 1 Regression of 850 hPa winds (m s^{-1}) during JJA(1) with respect to the normalized D(0)JF(1) Niño3.4 index in **a** observations and **b** CMIP MME. **c** D(0)JF(1) Niño3.4 index regressed NWPAC anomalies during

JJA(1) in observations (red dashed line), CMIP MME, and 47 CMIP models. Numbers 0 and 1–47 on abscissa of (c) represent the CMIP MME and model numbers listed in Table 1, respectively

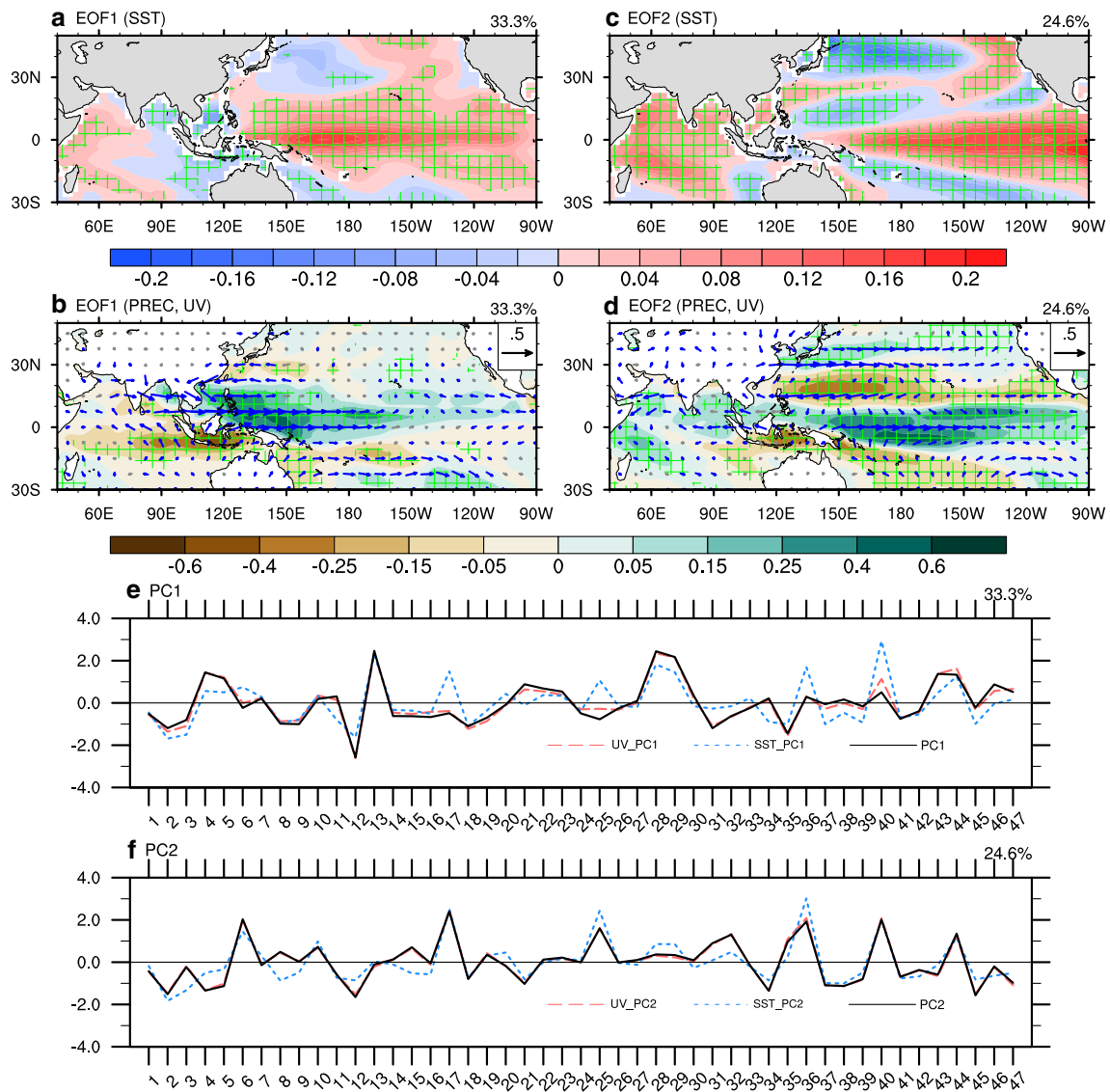


Fig. 2 Regression of D(0)JF(1) Niño3.4 index regressed SST (shaded, °C), 850 hPa wind (vector, m s⁻¹), and precipitation (shaded, mm) anomalies during JJA(1) with respect to the normalized PC1 (top left panels, **a**, **b**) and PC2 (top right panels, **c**, **d**) of intermodel EOF in 47 CMIP models. Green lattices and blue vectors indicate that the significant

level reaches 90%. Also shown are the standardized leading two PCs: **e** PC1 and **f** PC2 (black solid lines), as well as the leading PCs for intermodel SVD of D(0)JF(1) Niño3.4 index regressed 850 hPa wind (red dashed lines) and SST anomalies (blue dotted lines). The explained variances are given at the top right of panels

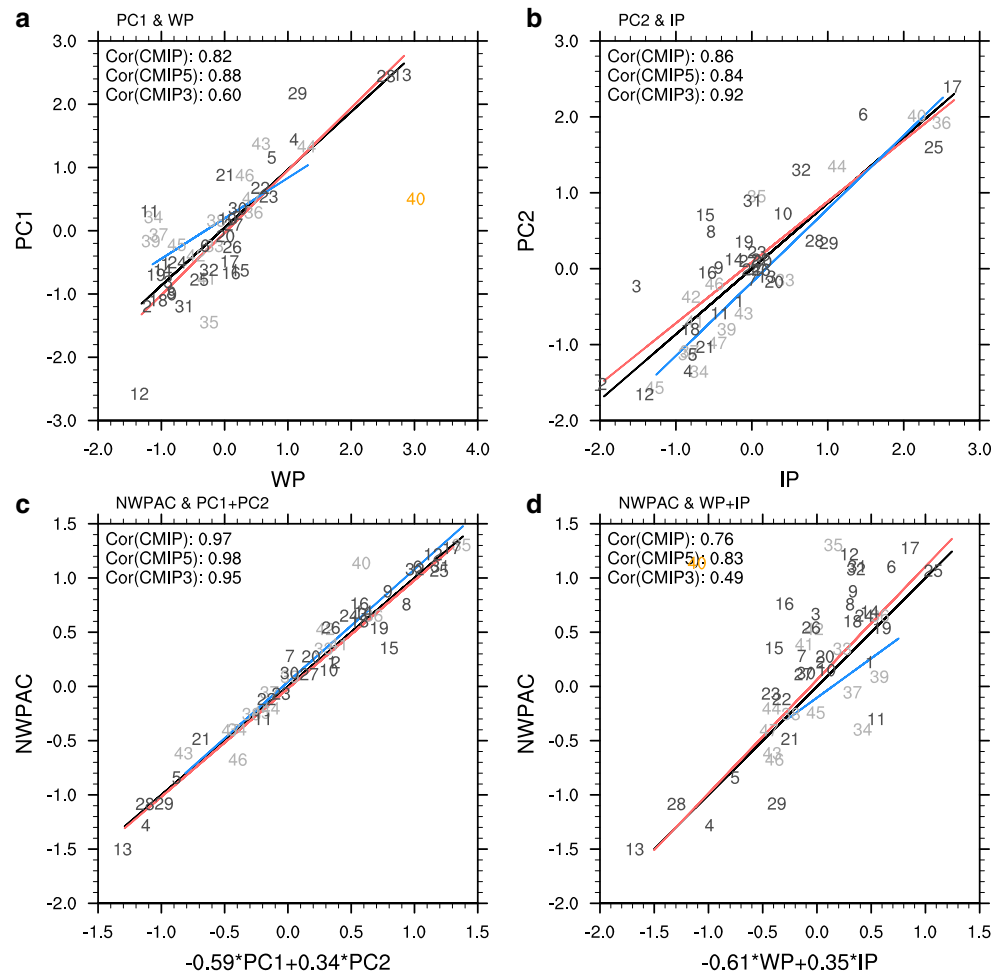
mode, the anomalous cyclone indicates the weaker simulation of NWPAC, and model with higher (lower) PC1 value or warmer (colder) SST anomalies over the equatorial WP tends to have a poorer (better) simulation of NWPAC.

The second intermodel EOF mode (EOF2), explaining 24.6% of total variance, displays a meridional tripole structure of circulation anomalies: The cyclonic wind anomalies are mainly concentrated over the tropical WP, an anomalous cyclone north of 30° N covers almost the whole north Pacific, and the NWPAC appears between them (Fig. 2d). The SST anomalies feature a tripole pattern over the Indo-Pacific sector, with warming over the TIO and equatorial CEP, and cooling over the NWP (Fig. 2c). The PC2 is highly correlated

with SST anomalies in above three regions at 0.86, which reaches 99% significant level (Fig. 3b). Note that the correlation coefficients between PC2 and SST anomalies in any one or two of the three regions are lower than that using all three regions (Table 2). As a result, model with higher (lower) PC2 value or stronger (weaker) SST anomalies over the TIO, CEP, and NWP indicates a stronger (weaker) NWPAC.

Based on multivariate regression, the diversity of NWP circulation anomalies during post-ENSO is almost totally attributed to the contribution of the leading two intermodel EOF modes (Fig. 3c), which are tightly linked to the SST biases over the equatorial WP and Indo-Pacific sector (Fig. 3d). The leading PCs and SST biases could explain 94.4% and 58.3%

Fig. 3 Scatter diagram of **a** PC1 (ordinate) and D(0)JF(1) Niño3.4 index regressed SST anomalies over the equatorial WP (abscissa; 10° S–10° N, 150° E–170° W); **b** PC2 (ordinate) and D(0)JF(1) Niño3.4 index regressed SST anomalies over the Indo-Pacific sector (abscissa); **c** original NWPAC intensity (ordinate) and NWPAC intensity built by PC1 and PC2 (abscissa) based on multivariate regression; and **d** original NWPAC intensity (ordinate) and NWPAC intensity built by D(0)JF(1) Niño3.4 index regressed SST anomalies over the equatorial WP and Indo-Pacific sector (abscissa) based on multivariate regression. The SST anomalies over the Indo-Pacific sector are calculated as the sum of equatorial CEP (5° S–5° N, 170° W–120° W) and TIO (20° S–20° N, 40°–100° E) warming minus NWP (10°–20° N, 130° E–180°) cooling. Numbers represent the model numbers listed in Table 1. The blue, red, and black lines are the best fit lines for the scatters of CMIP3, CMIP5, and all CMIP models, respectively. The correlation coefficients of CMIP3, CMIP5, and all CMIP models are on the top corner of each figure



of intermodel variance for NWP circulation anomalies, respectively. We also apply an intermodel singular value decomposition (SVD) analysis between NWPAC biases (10° S–40° N, 90° E–170° W) and SST biases (20° S–20° N, 40° E–90° W), and the leading PCs of SVD analysis are highly consistent with that of EOF analysis (Fig. 2e, f), confirming the close relationship between SST and NWPAC biases.

3.2 Role of SST biases

NWP circulation is sensitive to the tropical ocean status, and there are two views to understand the involved dynamic processes. On one hand, the anomalous atmospheric heating caused by SST anomalies induces NWP circulation anomalies following Gill-response mechanism (Wang et al. 2000; Xie et al. 2009; Fan et al. 2013; Karori et al. 2013; Chen et al. 2016). On the other hand, tropical SST anomalies drive the adjustment of large-scale tropical circulation, including Walker and Hadley circulation, which leads to anomalous NWP circulation (Wu et al. 2009a; Wu et al. 2009b; Chung et al. 2011; Chen and Zhou 2014; Gong et al. 2018b). Thus, the possible role of SST biases affecting NWPAC biases is

analyzed in this subsection in order to investigate how these two aspects work in first two EOF modes.

Figure 4a shows the PC1 regressed ENSO-related 200 hPa geopotential height and wind anomalies during JJA(1). Owing to the wet anomalies induced by the equatorial WP warming, geopotential height anomalies display a Matsuno-Gill (Matsuno 1966; Gill 1980) pattern, and a pair of Rossby waves are triggered to the east as two off-equatorial maximum centers (Figs. 2b and 4a). Upper-level easterly wind anomalies dominate the Maritime Continent (MC) region, and an anomalous lower-level cyclone is triggered at the tropical NWP as a direct Rossby wave response to the positive rainfall anomalies there (Fig. 2b), which are accompanied by the local convergence (divergence) at lower (upper) levels (Fig. 5a, b).

The PC2 regressed ENSO-related 200 hPa geopotential height anomalies feature an off-equatorial maximum on either side of the equator over the CEP and an equatorial maximum to the east over the TIO, as the Matsuno-Gill (Matsuno 1966; Gill 1980) patterns anchored by the CEP and TIO warming, respectively (Fig. 4b). The CEP (TIO) warming affects NWPAC through Rossby (Kelvin) wave-induced divergence mechanism as observational La Niña cases (Chen et al. 2017;

Table 2 Correlation coefficients between PC2 and SST anomalies in any one, two, or all of the three regions: TIO, CEP, and NWP

TIO	CEP	NWP	TIO + CEP	TIO-NWP	CEP-NWP	TIO + CEP-NWP
0.73	0.68	-0.51	0.78	0.80	0.83	0.86

Tao et al. 2017) and slow decaying El Niño cases (Jiang et al. 2019). The associated precipitation and large-scale circulation anomalies exhibit tripole patterns: the negative rainfall anomalies with lower- (upper-) level convergence (divergence) are clearly seen over the NWP and MC, and they are in conjunction with the positive rainfall anomalies and lower- (upper-) level divergence (convergence) over the TIO and central Pacific (Figs. 2d and 5c, d). Further, to examine the physical mechanism involved in leading mode-related SST biases affecting the simulation of NWP circulation, solutions to atmospheric general circulation model (AGCM) are considered in the next subsection.

3.3 Solutions to AGCM

Six simulations are conducted with different boundary conditions by using the Max Plank Institute for Meteorology AGCM (ECHAM5.3.2; Roeckner et al. 2003), and we adopt a version with triangular truncation at zonal wavenumber 63 (T63; equivalent to 1.9° horizontal resolution) and 31 vertical levels extending to 10 hPa. In control run (hereafter CTL run), the model is forced by the CMIP multimodel ensemble (MME) monthly climatology of SST for 1970–2009. The composite of SST anomalies during post-ENSO summer for the positive PC1 and PC2 value (PC1+ and PC2+; above 0.75) models added to the CTL run in the WP and Indo-pacific sector (hereafter WP and IP run), respectively, to denote the effect of leading mode-related SST biases. Note that an El Niño (La Niña) event is defined as the normalized D(0)JF(1) Niño3.4 index is above 0.75 (below -0.75), and the composite maps are calculated as the difference between El Niño and La Niña events for positive PC value models. The composite results for PC1+ and PC2+ models highly resemble the leading modes of SST, 850 hPa wind, and precipitation anomalies (Figs. 2a–d and 6a–d). Besides, to obtain the relative contribution of SST anomalies in the TIO, CEP, and NWP to the

simulation of NWPAC for PC2+ models, three additional experiments (hereafter TIO, CEP, and NWP run) are conducted. In all experiments, the SST is kept constant in time and the model is integrated for 40 years, and last 30 years’ mean results for JJA are analyzed. The detailed information of simulations is listed in Table 3.

To document the equatorial WP warming in EOF1 affects NWP circulation biases. The difference of simulated rainfall and 850 hPa wind anomalies between WP run and CTL run during JJA(1) is shown in Fig. 6c. The features of EOF1 are reasonably captured by WP run, although the model results are stronger than PC1+ models (Fig. 6b, c). The response of large-scale circulation is also well reproduced (figures not shown), and the equatorial WP warming enhances local convection with lower- (upper-) level convergence (divergence), inducing wet anomalies there. In response to the positive precipitation anomalies over the WP, a pair of Rossby waves are triggered to the west following Gill-response mechanism, and an anomalous cyclone appears over the tropical NWP (Fig. 6c).

For EOF2, Fig. 6f presents the difference of simulated rainfall and 850 hPa wind anomalies between IP run and CTL run during JJA(1). Model well reproduces the features of EOF2, as the rainfall and circulation anomalies over the Indo-Pacific sector (Fig. 6e, f), confirming the importance of SST anomalies over the Indo-Pacific sector affecting the simulation of NWP circulation. The TIO (CEP) warming induces local wet anomalies, which trigger eastward (westward) Kelvin (Rossby) wave, resulting the adjustment of large-scale circulation (figures not shown). The resultant lower- (upper-) level divergence (convergence) suppresses convection over the MC and NWP, inducing the dry anomalies there (Fig. 6f). The anomalous NWPAC is triggered as a Rossby wave response to the local negative precipitation anomalies. Besides, the NWP cooling contributes to development of NWPAC via the positive thermodynamic feedback between local SST and

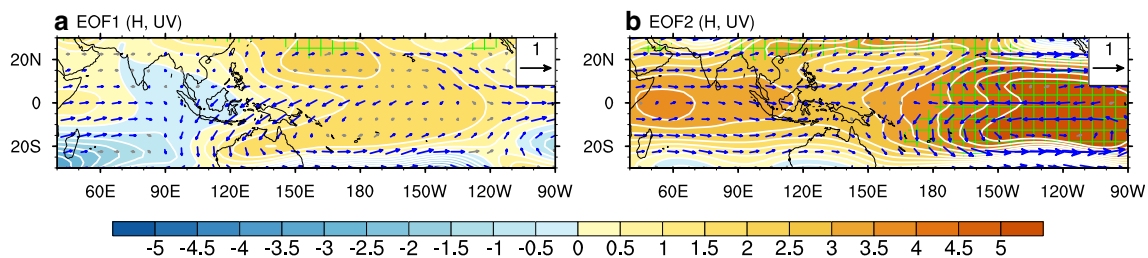


Fig. 4 Regression of D(0)JF(1) Niño3.4 index regressed 200 hPa geopotential height (shaded, °C) and wind anomalies (vector, m s⁻¹) during JJA(1) with respect to the normalized **a** PC1 and **b** PC2. Green lattices and blue vectors indicate significant level reaches 90%

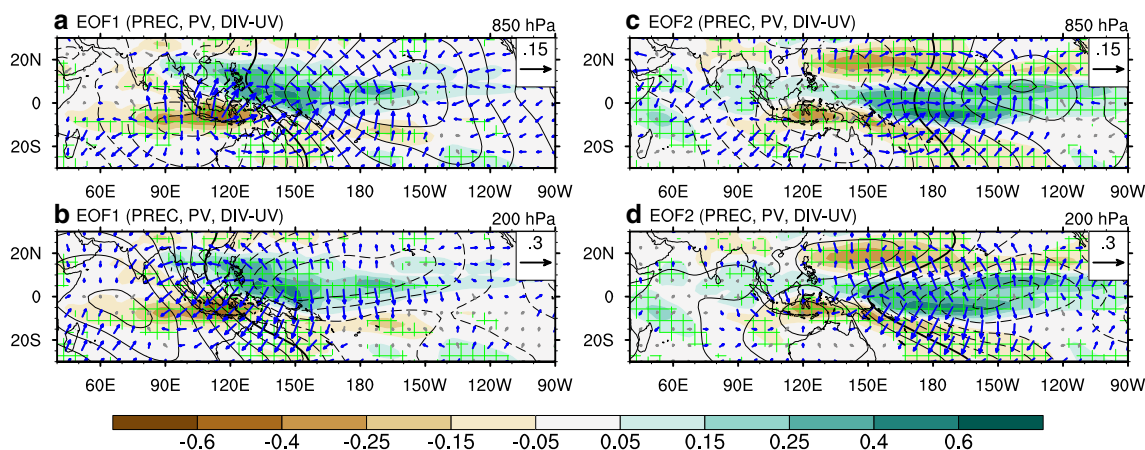


Fig. 5 Regression of D(0)JF(1) Niño3.4 index regressed 850 hPa potential velocity (contour, $10^6 \text{ m}^2 \text{ s}^{-1}$) and divergent wind (vector, m s^{-1}), 200 hPa potential velocity (contour, $10^6 \text{ m}^2 \text{ s}^{-1}$) and divergent wind (vector, m s^{-1}), and precipitation anomalies (shaded, mm) during

JJA(1) with respect to the normalized PC1 (left panels, **a, b**) and PC2 (right panels, **c, d**). Green lattices for precipitation and blue vectors for winds indicate significant level reaches 90%

circulation anomalies (Wang et al. 2000; Wang and Zhang 2002; Wu et al. 2010; Wang et al. 2013; Xiang et al. 2013; Wu et al. 2017a).

Furthermore, the relative contribution of SST anomalies in the three regions of Indo-Pacific sector to the simulation of

NWPAC is explored, and the NWPAC intensity in the four experiments and PC2+ models is shown in Table 4. Consistent with the conclusion of Table 2, the SST anomalies in all three regions have crucial contribution to the NWP circulation biases, and the NWPAC is strongest if SST anomalies over

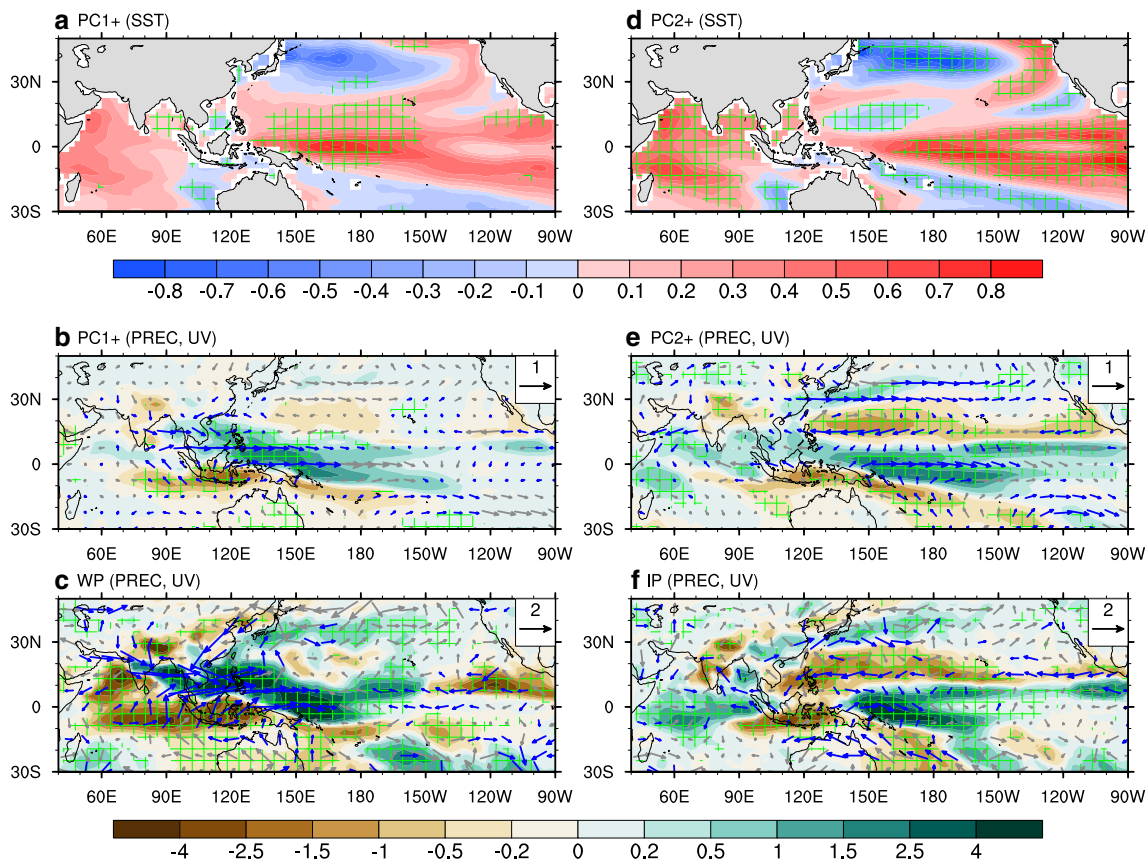


Fig. 6 Composite of SST (shaded, $^{\circ}\text{C}$), 850 hPa winds (vector, m s^{-1}), and precipitation (shaded, mm) during JJA(1) for PC1+ models (top left panels, **a, b**) and PC2+ models (top right panels, **d, e**). Simulated 850 hPa

wind (vector; m s^{-1}) and precipitation (shaded; mm) anomalies during JJA(1) for **c** WP minus CTL run and **f** IP minus CTL run. Green lattices and blue vectors indicate significant level reaches 90%

Table 3 List of the six ECHAM5.3.2 simulations: CTL, WP, TIO, CEP, NWP, and IP run

Simulation	SST forcing field	Integration
CTL run	CMIP MME global climatological SST for 1970–2009	40 years
WP run	Added composite of positive SST anomalies for the positive PC1 value models over the WP (20° S–20° N, 120° E–150° W) in Fig. 6a to CTL run from June to August	40 years
TIO run	Added composite of positive SST anomalies for the positive PC2 value models over the TIO (20° S–20° N, 40°–120° E) in Fig. 6d to CTL run from June to August	40 years
CEP run	Added composite of positive SST anomalies for the positive PC2 value models over the CEP (20° S–20° N, 140° E–70° W) in Fig. 6d to CTL run from June to August	40 years
NWP run	Added composite of negative SST anomalies for the positive PC2 value models over the NWP (5°–25° N, 120° E–160° W) in Fig. 6d to CTL run from June to August	40 years
IP run	Added the SST anomalies in TIO, CEP, and NWP run together to CTL run	40 years

the whole Indo-Pacific sector are included, as conducted by IP run. Besides, the NWPAC in CEP run is stronger than the other two runs, indicating the dominant role of CEP warming. The NWP cooling has the least contribution, and it could be attributed to the fast decaying SST anomalies there (figures not shown). Note that the simulated precipitation and circulation anomalies in WP and IP run are stronger than the relevant composite results (Fig. 6b, c, e, f, and Table 4), probably due to that the atmospheric feedback to SST could not be simulated by AGCM.

4 Summary

Based on an intermodel EOF analysis, this study has investigated the dominant modes of NWP circulation anomalies during post-ENSO summer and their SST dependence involved in 47 CMIP models. The main findings are summarized as follows.

The first intermodel EOF mode, explaining 33.3% of total intermodel variance, features an anomalous cyclone over the tropical NWP (Fig. 2b). Positive SST anomalies can be seen over the equatorial WP (Fig. 2a), and model with warmer (colder) SST anomalies over the equatorial WP tends to have a poorer (better) simulation of NWPAC (Fig. 3a). The equatorial WP warming enhances local convection with lower-(upper-) level convergence (divergence), and the anomalous NWP cyclone is a direct Rossby wave response to positive rainfall anomalies there (Figs. 4a and 5a, b). An AGCM is used and forced by adding positive SST anomalies over the WP to CMIP MME global climatological SST. Model results reproduce the EOF1 features, conforming the role of equatorial WP warming affecting the simulation of NWP circulation (Fig. 6c).

The second intermodel EOF mode explains 24.6% of total variance, and an anomalous anticyclone is captured over the NWP (Fig. 2d). The associated SST anomalies feature a tripole pattern over the Indo-Pacific sector, with warming over the TIO and equatorial CEP, and cooling over the NWP

(Fig. 2c). Model with stronger (weaker) SST anomalies over the TIO, CEP, and NWP indicates a stronger (weaker) NWPAC (Fig. 3b). The TIO (CEP) warming induces local wet anomalies, and the 200-hPa geopotential height anomalies there display the Matsuno-Gill pattern with eastward (westward) Kelvin (Rossby) wave, resulting the adjustment of large-scale circulation (Figs. 4b and 5c, d). The resultant lower- (upper-) level divergence (convergence) suppresses convection over the MC and NWP, inducing the anomalous NWPAC as a Rossby wave response. Besides, the NWP cooling contributes to development of NWPAC via positive thermodynamic feedback between local SST and circulation anomalies. Model results are consistent with EOF2 patterns, and emphasize the importance of SST anomalies over the Indo-Pacific contributing to simulation of NWPAC (Fig. 6f).

The unrealistic positive SST anomalies over the equatorial WP in EOF1 are related to the overly westward extension of simulated ENSO warm tongue, which can persist through JJA(1) (Tao et al. 2015a; Jiang et al. 2017; Tao et al. 2018). The overly westward extended ENSO warming originates from the excessive equatorial Pacific cold tongue in the models (Tao et al. 2018). On one hand, the cold SST biases increase the mean zonal SST gradient, and favor the development and persistence of WP warming via intensified warm zonal advection. On the other hand, the anomalous convection caused by ENSO-related warming is reduced, and the WP SST increase as more downward shortwave radiation. While, the EOF2-related Indo-Pacific SST patterns are highly controlled by ENSO amplitude and its decaying pace, which are determined by the intensity of subtropical cells via the adjustment of meridional and vertical advection (Tao et al. 2018).

Table 4 The NWPAC intensity (m s^{-1}) in PC2+ models, as well as TIO, CEP, NWP, and IP run

PC2+ models	TIO run	CEP run	NWP run	IP run
0.75	0.61	0.87	0.49	0.91

This study reveals the importance of intermodel diversity in Indo-Pacific SST anomalies during post-ENSO summer to NWP circulation. However, the obtained conclusions are not only limited to model biases, but also have some enlightenment for understanding how diversity of ENSO types and their evolution affects NWP circulation in observational cases. Besides, weakening NWPAC during post-ENSO summer under global warming is projected by CMIP5 MME result (Jiang et al. 2018; He et al. 2019), and they emphasized the weakening role of NWP thermodynamic feedback and TIO warming, respectively. So, how do the leading modes of NWP circulation and their SST dependence change under global warming? What mechanism is involved in processes between SST and NWP circulation? All these issues deserve to further study in the future.

Acknowledgments We acknowledge the World Climate Research Program's Working Group on Coupled Modeling, which is responsible for CMIP, and we thank the climate modeling groups (listed in Table 1 of this paper) for producing and making available their model output. For CMIP, the U.S. Department of Energy's Program for Climate Model Diagnosis and Intercomparison provides coordinating support and led development of software infrastructure in partnership with the Global Organization for Earth System Science Portals. We thank two anonymous reviewers as well as the editor for their useful comments. This work was supported by the National Natural Science Foundation of China (41425019, 41831175, 41721004, and 41705068), the China Postdoctoral Science Foundation (2016LH0005 and 2016M600116), and the Natural Science Foundation of Guangdong Province (2016A030310009).

References

- Bellenger H, Guilyardi E, Leloup J, Lengaigne M, Vialard J (2014) ENSO representation in climate models: from CMIP3 to CMIP5. *Clim Dyn* 42(7–8):1999–2018. <https://doi.org/10.1007/s00382-013-1783-z>
- Chang CP, Zhang Y, Li T (2000) Interannual and interdecadal variations of the East Asian summer monsoon and tropical Pacific SSTs. Part II: meridional structure of the monsoon. *J Clim* 13(24):4326–4340. [https://doi.org/10.1175/1520-0442\(2000\)013<4326:iaivot>2.0.co;2](https://doi.org/10.1175/1520-0442(2000)013<4326:iaivot>2.0.co;2)
- Chen X, Zhou T (2014) Relative role of tropical SST forcing in the 1990s periodicity change of the Pacific-Japan pattern interannual variability. *J Geophys Res-Atmos* 119(23):2014JD022064. <https://doi.org/10.1002/2014jd022064>
- Chen M, Xie P, Janowiak JE, Arkin PA (2002) Global land precipitation: a 50-yr monthly analysis based on gauge observations. *J Hydrometeorol* 3(3):249–266. [https://doi.org/10.1175/1525-7541\(2002\)003<0249:glpaym>2.0.co;2](https://doi.org/10.1175/1525-7541(2002)003<0249:glpaym>2.0.co;2)
- Chen Z, Wen Z, Wu R, Zhao P, Cao J (2014) Influence of two types of El Niños on the East Asian climate during boreal summer: a numerical study. *Clim Dyn* 43(1–2):469–481. <https://doi.org/10.1007/s00382-013-1943-1>
- Chen Z, Wen Z, Wu R, Lin X, Wang J (2016) Relative importance of tropical SST anomalies in maintaining the Western North Pacific anomalous anticyclone during El Niño to La Niña transition years. *Clim Dyn* 46(3):1027–1041. <https://doi.org/10.1007/s00382-015-2630-1>
- Chen Z, Wen Z, Wu R, Du Y (2017) Roles of tropical SST anomalies in modulating the western north Pacific anomalous cyclone during strong La Niña decaying years. *Clim Dyn* 49(1):633–647. <https://doi.org/10.1007/s00382-016-3364-4>
- Chiang JCH, Sobel AH (2002) Tropical tropospheric temperature variations caused by ENSO and their influence on the remote tropical climate. *J Clim* 15(18):2616–2631. [https://doi.org/10.1175/1520-0442\(2002\)015<2616:ttvcb>2.0.co;2](https://doi.org/10.1175/1520-0442(2002)015<2616:ttvcb>2.0.co;2)
- Chowdary JS, Gnanaseelan C (2007) Basin-wide warming of the Indian Ocean during El Niño and Indian Ocean dipole years. *Int J Climatol* 27(11):1421–1438. <https://doi.org/10.1002/joc.1482>
- Chowdary JS, Xie SP, Luo JJ, Hafner J, Behera S, Masumoto Y, Yamagata T (2011) Predictability of Northwest Pacific climate during summer and the role of the tropical Indian Ocean. *Clim Dyn* 36(3–4):607–621. <https://doi.org/10.1007/s00382-009-0686-5>
- Chowdary JS, Parekh A, Kakatkar R, Gnanaseelan C, Srinivas G, Singh P, Roxy MK (2016) Tropical Indian Ocean response to the decay phase of El Niño in a coupled model and associated changes in south and east-Asian summer monsoon circulation and rainfall. *Clim Dyn* 47(3):831–844. <https://doi.org/10.1007/s00382-015-2874-9>
- Chung P-H, Sui C-H, Li T (2011) Interannual relationships between the tropical sea surface temperature and summertime subtropical anticyclone over the western North Pacific. *J Geophys Res-Atmos* 116(D13):D13111. <https://doi.org/10.1029/2010jd015554>
- Dong D, Huang G, Tao W, Wu R, Hu K, Li C (2018) Interannual variation of precipitation over the Hengduan Mountains during rainy season. *Int J Climatol* 38(4):2112–2125. <https://doi.org/10.1002/joc.5321>
- Du Y, Xie SP, Huang G, Hu K (2009) Role of air-sea interaction in the long persistence of El Niño-induced north Indian Ocean warming. *J Clim* 22(8):2023–2038
- Fan L, Shin S-I, Liu Q, Liu Z (2013) Relative importance of tropical SST anomalies in forcing East Asian summer monsoon circulation. *Geophys Res Lett* 40(10):2471–2477. <https://doi.org/10.1002/grl.50494>
- Gill AE (1980) Some simple solutions for heat-induced tropical circulation. *Q J R Meteorol Soc* 106(449):447–462. <https://doi.org/10.1256/smsqj.44904>
- Gong Z, Dogar MM, Qiao S, Hu P, Feng G (2018a) Assessment and correction of BCC_CSM's performance in capturing leading modes of summer precipitation over North Asia. *Int J Climatol* 38(5):2201–2214. <https://doi.org/10.1002/joc.5327>
- Gong Z, Feng G, Dogar MM, Huang G (2018b) The possible physical mechanism for the EAP-SR co-action. *Clim Dyn* 51(4):1499–1516. <https://doi.org/10.1007/s00382-017-3967-4>
- He C, Zhou T, Li T (2019) Weakened anomalous western North Pacific anticyclone during an El Niño-decaying summer under a warmer climate: dominant role of the weakened impact of the tropical Indian Ocean on the atmosphere. *J Clim* 32(1):213–230. <https://doi.org/10.1175/jcli-d-18-0033.1>
- Hu K, Huang G, Wu R (2012) A strengthened influence of ENSO on August high temperature extremes over the southern Yangtze River valley since the late 1980s. *J Clim* 26(7):2205–2221. <https://doi.org/10.1175/jcli-d-12-00277.1>
- Hu K, Huang G, Zheng X-T, Xie S-P, Qu X, Du Y, Liu L (2014) Interdecadal variations in ENSO influences on Northwest Pacific-East Asian early summertime climate simulated in CMIP5 models. *J Clim* 27(15):5982–5998. <https://doi.org/10.1175/jcli-d-13-00268.1>
- Hu K, Xie S-P, Huang G (2017) Orographically anchored El Niño effect on summer rainfall in Central China. *J Clim* 30(24):10037–10045. <https://doi.org/10.1175/jcli-d-17-0312.1>
- Jiang W, Huang G, Hu K, Wu R, Gong H, Chen X, Tao W (2017) Diverse relationship between ENSO and the Northwest Pacific summer climate among CMIP5 models: dependence on the ENSO decay pace. *J Clim* 30(1):109–127. <https://doi.org/10.1175/jcli-d-16-0365.1>
- Jiang W, Huang G, Huang P, Hu K (2018) Weakening of Northwest Pacific anticyclone anomalies during post-El Niño summers under

- global warming. *J Clim* 31(9):3539–3555. <https://doi.org/10.1175/jcli-d-17-0613.1>
- Jiang W, Huang G, Huang P, Wu R, Hu K, Chen W (2019) Northwest Pacific anticyclonic anomalies during post-El Niño summers determined by the pace of El Niño decay. *J Clim* 32(12):3487–3503. <https://doi.org/10.1175/jcli-d-18-0793.1>
- Kalnay E, Kanamitsu M, Kistler R, Collins W, Deaven D, Gandin L, Iredell M, Saha S, White G, Woollen J, Zhu Y, Chelliah M, Ebisuzaki W, Higgins W, Janowiak J, Mo KC, Ropelewski C, Wang J, Leetmaa A, Reynolds R, Jenne R, Joseph D (1996) The NCEP/NCAR 40-year reanalysis project. *Bull Am Meteorol Soc* 77(3):437–471. [https://doi.org/10.1175/1520-0477\(1996\)077<0437:tmyrp>2.0.co;2](https://doi.org/10.1175/1520-0477(1996)077<0437:tmyrp>2.0.co;2)
- Karori MA, Li JP, Jin FF (2013) The asymmetric influence of the two types of El Niño and La Niña on summer rainfall over Southeast China. *J Clim* 26(13):4567–4582. <https://doi.org/10.1175/jcli-d-12-00324.1>
- Klein SA, Soden BJ, Lau N-C (1999) Remote sea surface temperature variations during ENSO: evidence for a tropical atmospheric bridge. *J Clim* 12(4):917–932. [https://doi.org/10.1175/1520-0442\(1999\)012<0917:rsstvd>2.0.co;2](https://doi.org/10.1175/1520-0442(1999)012<0917:rsstvd>2.0.co;2)
- Lau NC, Nath MJ (1996) The role of the “atmospheric bridge” in linking tropical Pacific ENSO events to extratropical SST anomalies. *J Clim* 9:2036–2057
- Matsuno T (1966) Quasi-geostrophic motions in the equatorial area. *J Meteor Soc Japan* 44(1):25–43
- North GR, Bell TL, Cahalan RF, Moeng FJ (1982) Sampling errors in the estimation of empirical orthogonal functions. *Mon Weather Rev* 110(7):699–706. [https://doi.org/10.1175/1520-0493\(1982\)110<0699:seiteo>2.0.co;2](https://doi.org/10.1175/1520-0493(1982)110<0699:seiteo>2.0.co;2)
- Rayner NA, Parker DE, Horton EB, Folland CK, Alexander LV, Rowell DP, Kent EC, Kaplan A (2003) Global analyses of sea surface temperature, sea ice, and night marine air temperature since the late nineteenth century. *J Geophys Res-Atmos* 108(D14):4407. <https://doi.org/10.1029/2002jd002670>
- Roeckner E, Bäuml G, Bonaventura L, Brokopf R, Esch M, Giorgetta M, Hagemann S, Kirchner I, Komblueh L, Manzini E, Rhodin A, Schlese U, Schulzweida U, Tompkins A (2003) Atmospheric general circulation model ECHAM5: part I. Max-Planck-Institut für Meteorologie Rep 349:140
- Stuecker MF, Timmermann A, Jin F-F, McGregor S, Ren H-L (2013) A combination mode of the annual cycle and the El Niño/Southern Oscillation. *Nat Geosci* 6(7):540–544. <https://doi.org/10.1038/geo1826>
- Stuecker MF, Jin F-F, Timmermann A, McGregor S (2015) Combination mode dynamics of the anomalous Northwest Pacific anticyclone. *J Clim* 28(3):1093–1111. <https://doi.org/10.1175/jcli-d-14-00225.1>
- Tao W, Huang G, Hu K, Qu X, Wen G, Gong Y (2014) Different influences of two types of El Niños on the Indian Ocean SST variations. *Theor Appl Climatol* 117(3–4):475–484. <https://doi.org/10.1007/s00704-013-1022-x>
- Tao W, Huang G, Hu K, Gong H, Wen G, Liu L (2015a) A study of biases in simulation of the Indian Ocean basin mode and its capacitor effect in CMIP3/CMIP5 models. *Clim Dyn* 46(1):205–226. <https://doi.org/10.1007/s00382-015-2579-0>
- Tao W, Huang G, Hu K, Qu X, Wen G, Gong H (2015b) Interdecadal modulation of ENSO teleconnections to the Indian Ocean Basin mode and their relationship under global warming in CMIP5 models. *Int J Climatol* 35(3):391–407. <https://doi.org/10.1002/joc.3987>
- Tao W, Huang G, Wu R, Hu K, Wang P, Chen D (2017) Asymmetry in summertime atmospheric circulation anomalies over the northwest Pacific during decaying phase of El Niño and La Niña. *Clim Dyn* 49(5):2007–2023. <https://doi.org/10.1007/s00382-016-3432-9>
- Tao W, Huang G, Wu R, Hu K, Wang P, Gong H (2018) Origins of biases in CMIP5 models simulating Northwest Pacific summertime atmospheric circulation anomalies during the decaying phase of ENSO. *J Clim* 31(14):5707–5729. <https://doi.org/10.1175/jcli-d-17-0289.1>
- Wang B, Fan Z (1999) Choice of south Asian summer monsoon indices. *Bull Am Meteorol Soc* 80(4):629–638. [https://doi.org/10.1175/1520-0477\(1999\)080<0629:cosasm>2.0.co;2](https://doi.org/10.1175/1520-0477(1999)080<0629:cosasm>2.0.co;2)
- Wang B, Zhang Q (2002) Pacific-east Asian teleconnection. Part II: how the Philippine Sea anomalous anticyclone is established during El Niño development. *J Clim* 15(22):3252–3265. [https://doi.org/10.1175/1520-0442\(2002\)015<3252:peatpi>2.0.co;2](https://doi.org/10.1175/1520-0442(2002)015<3252:peatpi>2.0.co;2)
- Wang B, Wu RG, Fu XH (2000) Pacific-East Asian teleconnection: how does ENSO affect East Asian climate? *J Clim* 13(9):1517–1536. [https://doi.org/10.1175/1520-0442\(2000\)013<1517:peathd>2.0.co;2](https://doi.org/10.1175/1520-0442(2000)013<1517:peathd>2.0.co;2)
- Wang B, Wu ZW, Li JP, Liu J, Chang CP, Ding YH, Wu GX (2008) How to measure the strength of the east Asian summer monsoon. *J Clim* 21(17):4449–4463. <https://doi.org/10.1175/2008jcli2183.1>
- Wang B, Xiang B, Lee J-Y (2013) Subtropical high predictability establishes a promising way for monsoon and tropical storm predictions. *Proc Natl Acad Sci* 110(8):2718–2722. <https://doi.org/10.1073/pnas.1214626110>
- Watanabe M, Jin F (2002) Role of Indian Ocean warming in the development of Philippine Sea anticyclone during ENSO. *Geophys Res Lett* 29(10):1478
- Wu R, Yeh S-W (2010) A further study of the tropical Indian Ocean asymmetric mode in boreal spring. *J Geophys Res-Atmos* 115(D8):D08101. <https://doi.org/10.1029/2009jd012999>
- Wu RG, Hu ZZ, Kirtman BP (2003) Evolution of ENSO-related rainfall anomalies in East Asia. *J Clim* 16(22):3742–3758. [https://doi.org/10.1175/1520-0442\(2003\)016<3742:eoerai>2.0.co;2](https://doi.org/10.1175/1520-0442(2003)016<3742:eoerai>2.0.co;2)
- Wu R, Kirtman BP, Krishnamurthy V (2008) An asymmetric mode of tropical Indian Ocean rainfall variability in boreal spring. *J Geophys Res-Atmos* 113(D5):D05104. <https://doi.org/10.1029/2007jd009316>
- Wu B, Zhou T, Li T (2009a) Seasonally evolving dominant interannual variability modes of east Asian climate*. *J Clim* 22(11):2992–3005. <https://doi.org/10.1175/2008jcli2710.1>
- Wu R, Wen Z, Yang S, Li Y (2009b) An interdecadal change in southern China summer rainfall around 1992/93. *J Clim* 23(9):2389–2403. <https://doi.org/10.1175/2009jcli3336.1>
- Wu B, Li T, Zhou T (2010) Relative contributions of the Indian Ocean and local SST anomalies to the maintenance of the Western North Pacific anomalous anticyclone during the El Niño decaying summer*. *J Clim* 23(11):2974–2986. <https://doi.org/10.1175/2010jcli3300.1>
- Wu B, Zhou T, Li T (2017a) Atmospheric dynamic and thermodynamic processes driving the Western North Pacific anomalous anticyclone during El Niño. Part I: maintenance mechanisms. *J Clim* 30(23):9621–9635. <https://doi.org/10.1175/jcli-d-16-0489.1>
- Wu B, Zhou T, Li T (2017b) Atmospheric dynamic and thermodynamic processes driving the Western North Pacific anomalous anticyclone during El Niño. Part II: formation processes. *J Clim* 30(23):9637–9650. <https://doi.org/10.1175/jcli-d-16-0495.1>
- Xiang B, Wang B, Yu W, Xu S (2013) How can anomalous western North Pacific subtropical high intensify in late summer? *Geophys Res Lett* 40(10):2349–2354. <https://doi.org/10.1002/grl.50431>
- Xie S-P, Zhou Z-Q (2017) Seasonal modulations of El Niño-related atmospheric variability: Indo-Western Pacific Ocean feedback. *J Clim* 30(9):3461–3472. <https://doi.org/10.1175/jcli-d-16-0713.1>
- Xie SP, Annamalai H, Schott FA, McCreary JP Jr (2002) Structure and mechanisms of south Indian ocean climate variability. *J Clim* 15(8):864–878
- Xie SP, Hu K, Hafner J, Tokinaga H, Du Y, Huang G, Sampe T (2009) Indian Ocean capacitor effect on Indo-western Pacific climate during the summer following El Niño. *J Clim* 22(3):730–747

- Xie S-P, Kosaka Y, Du Y, Hu K, Chowdary JS, Huang G (2016) Indo-western Pacific Ocean capacitor and coherent climate anomalies in post-ENSO summer: a review. *Adv Atmos Sci* 33(4):411–432. <https://doi.org/10.1007/s00376-015-5192-6>
- Yang J, Liu Q, Xie S, Liu Z, Wu L (2007) Impact of the Indian Ocean SST basin mode on the Asian summer monsoon. *Geophys Res Lett* 34(2):L02708. <https://doi.org/10.1029/2006gl028571>
- Yang J, Liu Q, Liu Z (2010) Linking observations of the Asian monsoon to the Indian Ocean SST: possible roles of Indian Ocean basin mode and dipole mode. *J Clim* 23(21):5889–5902. <https://doi.org/10.1175/2010jcli2962.1>
- Zhang RH, Sumi A, Kimoto M (1996) Impact of El Nino on the East Asian monsoon: a diagnostic study of the '86/87 and '91/92 events. *J Meteorol Soc Jpn* 74(1):49–62
- Zhang W, Li H, Stuecker MF, Jin F-F, Turner AG (2016) A new understanding of El Niño's impact over East Asia: dominance of the ENSO combination mode. *J Clim* 29(12):4347–4359. <https://doi.org/10.1175/jcli-d-15-0104.1>

Publisher's note Springer Nature remains neutral with regard to jurisdictional claims in published maps and institutional affiliations.